Applied Energy 282 (2021) 116152

Contents lists available at ScienceDirect

Applied Energy

journal homepage: www.elsevier.com/locate/apenergy

Offline optimal energy management strategies considering high dynamics in batteries and constraints on fuel cell system power rate: From analytical derivation to validation on test bench☆

Hujun Peng [a,*], Zhu Chen [a], Jianxiang Li [a], Kai Deng [a], Steffen Dirkes [b], Jonas Gottschalk [b], Cem Ünlübayir [c], Andreas Thul [a], Lars Löwenstein [d], Stefan Pischinger [b], Kay Hameyer [a]

[a] Institute of Electrical Machines (IEM), RWTH Aachen University, Germany
[b] Institute for Combustion Engines (VKA), RWTH Aachen University, Germany
[c] Chair for Electrochemical Energy Conversion and Storage Systems, Institute for Power Electronics and Electrical Drives (ISEA), RWTH Aachen University, Germany
[d] Siemens Mobility GmbH, Vienna, Austria

HIGHLIGHTS

- Fuel cell power rate as the control variable to directly limit the power dynamic.
- Offline PMP-based strategy considering dynamics in batteries and in the costate.
- Two-dimensional dynamic programming with R-C branches in batteries considered.
- Utilization of the specific consumption curve to implement soft constraint for DP.
- Validation of the accuracy of offline strategies based on measurement on the test bench.

ARTICLE INFO

Keywords:
Fuel cell hybrid vehicles
Offline energy management
Pontryagin's minimum principle
Dynamic programming
Experimental validation

ABSTRACT

For a fuel cell hybrid train, offline optimal energy management strategies using the Pontryagin's minimum principle and dynamic programming are developed and presented in this contribution. The dynamics in the voltages over various parallel resistance-capacitor branches in the batteries are considered. In addition, dynamic limitation of the fuel cell power is taken into account by choosing the fuel cell power rate as the control variable instead of the fuel cell power, as found so far in all literature with related topics. The correctness of the Pontryagin's minimum principle and the dynamic programming-based strategies are mutually validated. The corresponding results provide more precise references than the offline strategies without the resistance-capacitor branches in batteries taken into account. A damping factor is then introduced into the cost function to reduce unnecessary high dynamic oscillations of the operating points of the fuel cell system without compromising fuel economy. Finally, the results of the offline strategies are validated with measurements on the test bench at the Center for Mobile Propulsion of the RWTH Aachen University. Only a difference of 0.15% was determined between the measured and the offline calculated hydrogen consumption. .

1. Introduction

1.1. Background

Fuel cell-powered railway vehicles are a promising alternative to electrify railway transportation without high investment in the catenaries. Thereby, the fuel cell systems provide the average load, while the battery systems cover the high peak power during acceleration and regenerative braking phases. Alstom brought the world's first fuel cell hybrid trains to market, and they began service to replace diesel-driven

☆ This study is funded by the German Federal Ministry of Transport and Digital Infrastructure (BMVi) under the National Innovation Program Hydrogen and Fuel Cell Technology (NIP). The funding numbers are 03B10502B and 03B10502B2. The authors gratefully thank the support of Siemens AG, Ballard, and NIP.

* Corresponding author.
E-mail address: hujun.peng@iem.rwth-aachen.de (H. Peng).

https://doi.org/10.1016/j.apenergy.2020.116152
Received 26 July 2020; Received in revised form 6 October 2020; Accepted 28 October 2020

trains in Germany in 2018 [1]. Siemens is also working on a fuel cell variant of Mireo and cooperating with RWTH Aachen University to develop a universally applicable Hardware-in-the-Loop (HiL) test environment in which real components and their models can be integrated, further developed and evaluated [2]. As mentioned above, two energy sources are available to share the load power. Correspondingly, this degree of freedom of distributing the load power can be utilized to improve performance, including fuel economy and system durability. Particularly, the lifetime of fuel cell systems is sensitive to dynamic power changes [3]. Therefore, the power rate limits for fuel cell systems have to be considered [4].

1.2. Motivations and challenges

Regarding the design of the energy management strategy for fuel cell hybrid vehicles, there are three fundamental types: rule-based, methods based on local optimization, and methods based on global optimization [5]. The former two are real-time applicable due to much lower computational load compared to the global optimization-based method. The detailed design of the real-time strategies is either based on human heuristics or trained by the results from the global optimization-based method. In [6], the optimal operation modes of a rule-based strategy are extracted from the results of dynamic programming for a battery/capacitor hybrid vehicle. In [7], the parameters of a rule-based strategy are calibrated by dynamic programming for plug-in electric vehicles. In [8], dynamic programming is used to optimize the rule-based strategy to reduce the shift frequency. In [9], a scalable rule-based strategy is extracted from offline results, and it utilizes the convexity of the consumption curves of fuel cell systems. In [10], the costate in the proposed adaptive Pontryagin's minimum principle-based (APMP) strategy is analytically derived, also as initiated by the offline results. In [11], a model predictive controller (MPC) based on Pontryagin's minimum principle (PMP) is introduced for plug-in hybrid electric vehicles. Thereby, short-time speed forecasting is achieved by using a Markov chain model. Then, the shooting method is used to determine the correct initial costate for the preview time horizon. From the adaptivity aspect, the real-time strategies trained by using offline results are shown to be superior to those based on the human experience.

Furthermore, offline strategies provide reference results to evaluate online strategies' performance regarding the predefined cost function. In [12], dynamic programming is used as a benchmark to evaluate the implemented control algorithm's performance for series–parallel hybrid electric vehicles. In [13], The effect of fuel cell degradation on the hydrogen consumption is investigated by using dynamic programming to determine the optimal strategy with and without the consideration of fuel cell aging. In [14], the effect of component size on hydrogen consumption for a fuel cell hybrid excavator is analyzed by using PMP.

However, as found in the literature, the implemented offline strategies assume various simplifications, like neglecting the dynamics in the resistor–capacitor (R-C) branches or taking a constant value for the costate defined in PMP, which affects their rationality. Therefore, implementing offline strategies with high accuracy remains meaningful and challenging. Furthermore, the calculation effort should be economical.

1.3. Literature survey

In the offline strategies, dynamic programming and PMP are included. Dynamic programming is based on the Bellman's principle of optimality [15], and its results satisfy the sufficient conditions of optimal solutions, while the PMP-based strategy utilizes the optimal control theory, and its solution satisfies the necessary conditions of optimal solutions [16]. In [17], the sufficient two conditions for the PMP-based strategy to be global optimal are explained, with the cost function being convex, and the dynamic of state variable being concave.

Dynamic programming can solve nonlinear and non-convex problems with state and control constraints [18]. In dynamic programming, the control process is determined by iterative calculations minimizing the cost-to-go functions. However, the computational effort is exponentially proportional to the number of state and control variables, from which the problem named "*curse of dimensionality*" comes. In [19], two-dimensional dynamic programming is used to optimize the energy management of a fuel cell/battery/photovoltaic renewable energy system. However, the transition pattern succeeds in the form of point-to-point without mentioning the parallelization of the algorithm. In [20], the algorithm of two-dimensional dynamic programming is parallelized to reduce the computational time for fuel cell/battery/capacitor hybrid vehicles, with the state of charge (SoC) of the battery system and the capacitors as the state variables. However, the rate limits on the fuel cell system power are neglected, and a zero-order battery model without considering R-C branches is used. Benefiting from its optimality of solutions, dynamic programming can be utilized to optimize the component sizing, in order to realize tradeoff between system cost and fuel economy. In [21], two loops, with the inner loop using one-dimensional dynamic programming to determine the optimal power distribution under a given component sizing, and the outer loop changing the component parameters, are utilized to optimize the component sizing. However, dynamic programming is implemented under sparse discretization to reduce computational effort, and the parasite parameters of batteries are not considered. In [22], two-dimensional dynamic programming is implemented to calculate the best performance for each component sizing combination for fuel cell/battery/supercapacitor hybrid vehicles. Thereby, the SoC of batteries and capacitors are defined as the two state variables. However, the dynamic constraints on fuel cell systems and the parallel parasitic R-C branches are also not considered. In [23], two-dimensional dynamic programming is implemented with dynamic constraints considered and a dense discretization used. The algorithm is parallelized, and the transition in the discrete time-state space is not restricted to the pattern of point-to-point. However, the dynamics in the voltages over the R-C branches in batteries are not considered.

The PMP-based strategy is widely used to determine the offline strategy, with a lower computational load compared to dynamic programming. In [24,25], the offline PMP-based strategy is studied for fuel cell/battery hybrid vehicles. However, both dynamics in the costate and the R-C branches of batteries are not considered. In [26], real-time energy management is proposed for a parallel plug-in hybrid electric vehicle, as learned from offline results of the PMP-based strategy, whereby a simplified zero-order battery model is assumed. In [27], dynamics in the R-C branches are considered, in contrast to the majority of the PMP-related literature. However, the dependency of parasitic resistances and capacitors on the SoC and the dynamic of the costate are neglected. Furthermore, the dynamic constraint on fuel cell system power is not implemented. In [28], the fuel cell lifetime is considered by introducing a weighting factor to penalize the fuel cell system power dynamic. Thereby, a tradeoff between fuel consumption and the fuel cell stack lifetime is observed. However, the rate is not limited directly, which depends on the corresponding weighting factor. Furthermore, the PMP-based strategy can also be used to optimize the component sizing. In [29], the PMP strategy is used to minimize the total cost of energy consumption and battery degradation for the plug-in hybrid electric vehicles. Thereby, the battery modeling is simplified with the help of a zero-order equivalent circuit. In [30], the two-dimensional PMP-based algorithm is utilized to co-optimize the component sizing and the energy management strategy for a plug-in engine/battery/capacitor electrical bus. However, the dynamics because of R-C branches in batteries are not considered. In [31], a PMP-based strategy is used to optimize the component sizing with fuel economy and battery lifetime consumption. Thereby, the dynamic rate limits on the fuel cell system are taken into account by incorporating penalty factors. In [32], the PMP-based strategy is integrated with the velocity profile determination to realize coupled optimization between energy management and velocity

trajectory. Thereby, a two-dimensional PMP-based method, with the vehicle velocity as the second state variable, is proposed. However, the dynamic in costate and R-C branches are not considered. In [33], an implicit Hamiltonian minimization approach with penalty functions is developed to handle state constraints. However, battery modeling is simplified, limiting the optimality of its solutions. Summarily, in PMP-related works, no one has yet considered the dynamic constraints on the fuel cell system in combination with the dynamics in the costate, and the voltages over the R-C branches in batteries at the same time.

1.4. Objectives

The offline strategies are to be implemented, with constraints on fuel cell power dynamic, parasite parameters, and nonlinearity in battery modeling parameters considered. Both the PMP strategy and dynamic programming are to be implemented and validated because they have different advantages and drawbacks.

1.5. Main work

The following main contributions are included in this work:

- More accurate implementation of the PMP strategy than existing works. Thereby, the dynamics in the parasite voltages in batteries and the costate are fully considered. The dependency of parameters in the battery modeling on the SoC is taken into account. Furthermore, the power dynamic of fuel cell systems is chosen as the control variable to restrict its change rate instead of introducing a weighting factor in the cost function, as found in the literature.
- Implementation of the two-dimensional dynamic programming with algorithm parallelized. The parasite parameters and their dependency on SoC are also considered. The fuel cell power dynamic is defined as the control variable under the two-dimensional framework. Furthermore, the algorithm is parallelized to reduce computation time based on a semi-physical mechanism to initialize the cost function.
- Validation of the accuracy of the offline strategies based on the test bench measurement. Thereby, the offline results are regenerated and validated through measurements on the test bench located at the Center for Mobile Propulsion (CMP) of the RWTH Aachen University. A negligible difference of 0.15% in hydrogen consumption results between the calculated and measured values under the offline PMP strategy.

1.6. Paper organization

The system configuration necessary for analyzing the fuel economy of offline energy management is briefly explained in Section 2. The offline PMP-based strategy with dynamics in the R-C and the costate considered, is shown in detial in Section 3. The two-dimensional dynamic programming to handle dynamic constraints on fuel cell system power and the dynamics because of R-C branches in batteries is introduced in Section 4. The results of dynamic programming and the PMP-based strategy are validated by each other in Section 5. Thereby, a damping factor is introduced to analyze its effects on the fuel cell oscillation and fuel economy. In Section 6, the high power test bench is presented, and the accuracy of the offline strategy is validated with the help of measurements. In Section 7, conclusions and outlooks will be given.

2. Driveline

Similar to other approaches, that are found in literature, the SoC of battery and the train velocity are dynamically calculated, all other components are stationarily modeled by using lookup tables. Fig. 1 shows the structure of the whole simulation system. The model is built in

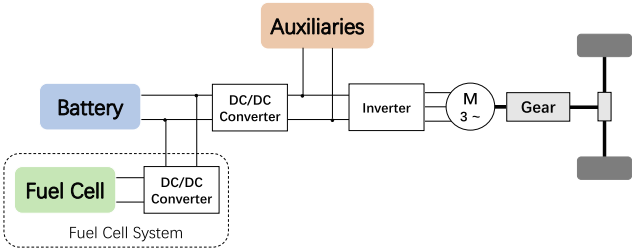

Fig. 1. Configuration of the driveline.

Simulink, as shown in Fig. 2. It corresponds to the power flow of a half train, which is proposed for the hardware-in-the-loop test. In [10], the modeling and parameters of each module are described in detail. In the simulation, the train line of Regional Express 1 between Aachen and Cologne is used as the driving cycle. Its velocity profile and slope change are displayed in Fig. 3. Firstly, a sequence of load power along the whole driving cycle is calculated in Simulink. In offline strategies, this load power profile would be utilized as one of the inputs, which is prior known. The other parameters related to the battery system and the fuel cell system, are explained in the following paragraphs.

2.1. Fuel cell system

For the fuel cell system, a proton exchange membrane fuel cell (PEMFC) is chosen, which combines the advantages of high system efficiency, high power density, good dynamic behavior, fast start-up and zero emission. The fuel cell system with a stated net power of 200 kW consists of two fuel cell stacks connected in parallel and several auxiliary components in the hydrogen, air and coolant path. The system efficiency is displayed in Fig. 4a and the polarization curve in Fig. 4b. The measured maximal system efficiency reaches 52% at 20% of full load and 44% at full load.

As mentioned in the introduction, the convexity of the hydrogen consumption curve in the considered operating range ensures the global optimality of PMP-based offline strategies. Fig. 5 shows this specific consumption curve, which is convex and can be mathematically formulated as

$$\dot{m}_{H_2}\left(\alpha \cdot P_{fc,1} + (1-\alpha)\cdot P_{fc,2}\right) < \alpha \cdot \dot{m}_{H_2}\left(P_{fc,1}\right) + (1-\alpha)\cdot \dot{m}_{H_2}\left(P_{fc,2}\right), \quad (1)$$

whereby the $\dot{m}_{H_2}$ represents the mass flow that is bijective to the entire fuel cell system's net output power, α is a factor between zero and one, $P_{fc,1}$ and $P_{fc,2}$ are two arbitrary working points of the fuel cell system.

In the next subsection, the modeling of the battery system will be explained.

2.2. Lithium-titanate battery system

For the battery system, Lithium-titanate battery cells (LTO) are chosen due to their long lifetime. Unlike the battery model used in most literature, an equivalent circuit, which includes three resistor–capacitor parallel branches, is utilized, as displayed in Fig. 6, to model the voltage drop over the entire internal resistance and relaxations precisely. The parameters of the parasite resistors and various time constants are displayed in Fig. 7 (c-h), which are fitted by measurement data. Fig. 7a shows the dependency of the battery's open-circuit voltage and Fig. 7b the resistance R_0 on the SoC and temperature. With the help of the implementation of active cooling within the simulation structure, the temperature is stabilized close to 25°C, so that the temperature dynamic can be neglected. The battery pack's rated voltage is 850 V and its capacity is approximately 200 kWh.

In the next section, the derivation and implementation of the offline PMP-based strategy will be introduced.

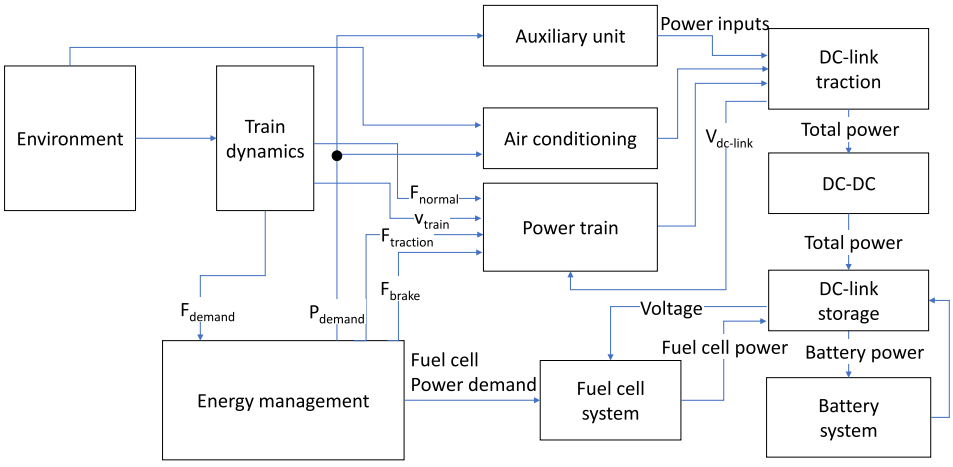

Fig. 2. Simulation structure of the hybrid train.

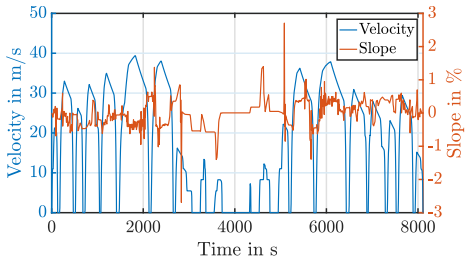

Fig. 3. The driving cycle between Aachen and Cologne has a distance of 145.8 km and a journey time of 8110 s.

3. Offline PMP with fuel cell system power rate as the control variable

Prior to the implementation of offline PMP-based strategy, the state, control, costate variables, disturbance signal and changeable parameters should be defined. Here, the SoC of batteries is chosen as the state variable, while the voltages over parasitic capacitors are set as changeable parameters and presented as V_1, V_2, V_3, respectively. Since the dynamics of SoC and these voltages are coupled by the same current, solely the state variable is controllable freely, and the others are defined as changeable parameters. The changing rate of fuel cell system power is set to be the control variable, and then, the fuel cell system power will be treated as another changeable parameter. The fuel cell system power is the integral of the control variable, as shown in Eq. (2):

$$P_{\mathrm{fc}}\left(t\right) = \int_0^t \dot{P}_{\mathrm{fc}}\left(\tau\right) d\tau. \tag{2}$$

In the following derivation processes, all the changeable parameters have zero derivations with respect to the state and the costate variable, because they have their own dynamic equations. As the core part of PMP-based strategies, the Hamiltonian function is defined in Eq. (3):

$$H\left(SoC, \dot{P}_{\mathrm{fc}}, \Delta t, P_{\mathrm{fc}}, \lambda, t\right) = \dot{m}_{\mathrm{H_2}}\left(P_{\mathrm{fc}}\left(t\right) + \frac{1}{2}\dot{P}_{\mathrm{fc}}\cdot\Delta t\right) + \lambda\left(t\right)\cdot\dot{SoC}\left(t\right), \tag{3}$$

whereby $\lambda(t)$ represents the costate variable with mass as the unit. $\dot{m}_{\mathrm{H_2}}$ describes the hydrogen mass flow, which depends on the fuel cell system

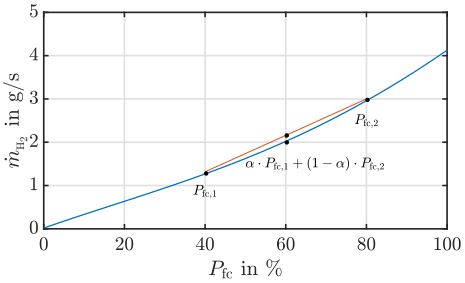

Fig. 5. Specific consumption curve of the entire fuel cell system.

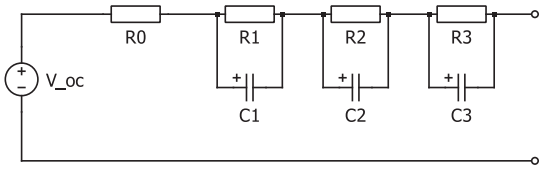

Fig. 6. The equivalent circuit including three R-C branches.

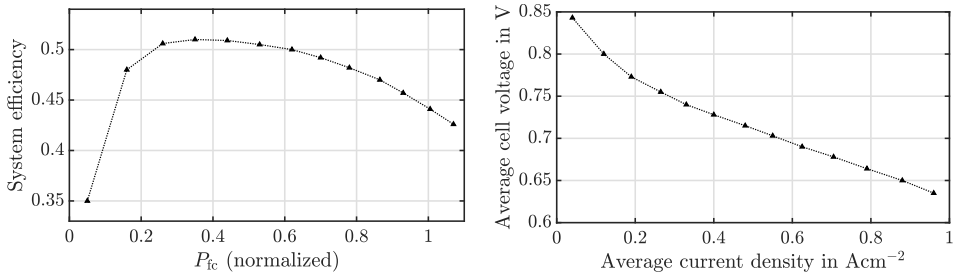

Fig. 4. Characteristic curves of fuel cell system: (a) System efficiency (b) Cell voltage dependent on current density.

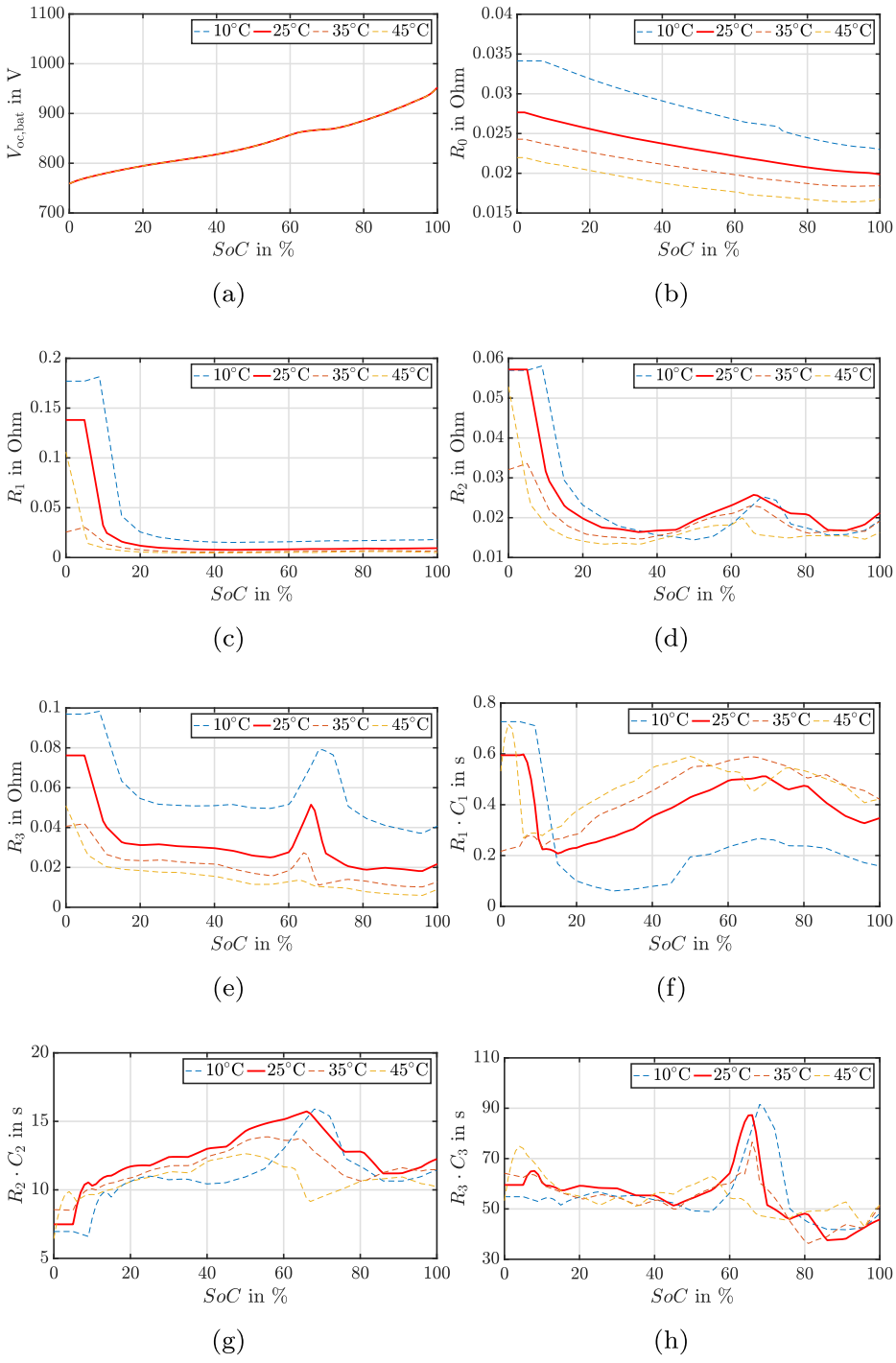

Fig. 7. Component parameters of the entire battery system: (a) The open-circuit voltage in Volt, (b) R_0 in Ohm, (c) R_1 in Ohm, (d) R_2 in Ohm, (e) R_3 in Ohm, (f) The time constant $R_1 \cdot C_1$ in seconds, (g) The time constant $R_2 \cdot C_2$ in seconds, (h) The time constant $R_3 \cdot C_3$ in seconds.

power. As a part of the cost function, it is necessary to estimate the hydrogen consumption rate, which depends on the averaged fuel cell system power in a time interval Δt. The average mass flow during the time interval $[t, t+\Delta t]$ can be calculated with the control variable $\dot{P}_{fc}$ and the actual fuel cell system power $P_{fc}(t)$ in Eq. (4):

$$\overline{P}_{fc} = P_{fc}\left(t\right) + \frac{1}{2}\dot{P}_{fc} \cdot \Delta t. \tag{4}$$

According to the theory of optimal control, the dynamic of the state is derived in Eq. (5):

$$\dot{SoC}\left(t\right) = \frac{\partial H\left(SoC, \dot{P}_{fc}, \Delta t, P_{fc}, \lambda, t\right)}{\partial \lambda} = -\frac{I_{bat}}{Q_{bat}}, \tag{5}$$

and the dynamic of the costate in Eq. (6):

$$\dot{\lambda}\left(t\right) = -\frac{\partial H\left(SoC, \dot{P}_{fc}, \Delta t, P_{fc}, \lambda, t\right)}{\partial SoC}. \tag{6}$$

As mentioned above, the variation of voltages over the parasitic capacitors is formulated in Eqs. (7)–(9):

$$\dot{V}_1\left(t\right) = \frac{I_{\text{bat}}}{C_1} - \frac{V_1}{C_1 \cdot R_1}, \tag{7}$$

$$\dot{V}_2\left(t\right) = \frac{I_{\text{bat}}}{C_2} - \frac{V_2}{C_2 \cdot R_2}, \tag{8}$$

$$\dot{V}_3(t) = \frac{I_{\text{bat}}}{C_3} - \frac{V_3}{C_3 \cdot R_3}, \tag{9}$$

where C_1, C_2, C_3 and R_1, R_2, R_3 are the values of parasitic capacitors and resistances, respectively.

By substituting the Hamiltonian function in Eq. (3) into Eq. (6), the dynamic of the costate is extended as shown in Eq. (10):

$$\dot{\lambda}\left(t\right) = -\frac{\partial \dot{m}_{\text{H}_2}}{\partial \dot{SoC}} - \lambda\left(t\right) \cdot \frac{\partial \dot{SoC}}{\partial SoC} = 0 - \lambda\left(t\right) \cdot \frac{\partial \dot{SoC}}{\partial SoC}. \tag{10}$$

Thereby, the derivation of $\dot{m}_{\text{H}_2}$ with respect to the state variable SoC is zero.

The current of battery I_{bat} depends on the averaged fuel cell system power and the load power as displayed in Eq. (11):

$$I_{\text{bat}} \cdot \left(V_{\text{oc,bat}} - \sum_{i=1}^{3} V_i - R_{0,\text{bat}} \cdot I_{\text{bat}}\right) = P_{\text{bat}} = P_{\text{load}} - \overline{P}_{\text{fc}}. \tag{11}$$

The difference between the open-circuit voltage and the sum of three voltages over capacitors is formulated in Eq. (12):

$$V_{\text{diff,bat}} = V_{\text{oc,bat}} - \sum_{i=1}^{3} V_i. \tag{12}$$

As the load power P_{load} and the averaged fuel cell system power $\overline{P}_{\text{fc}}$ are known, the battery current can be determined from Eq. (11) and results in Eq. (13):

$$I_{\text{bat}} = \frac{V_{\text{oc,bat}} - \sum_{i=1}^{3} V_i - \sqrt{\left(V_{\text{oc,bat}} - \sum_{i=1}^{3} V_i\right)^2 - 4\left(P_{\text{load}} - \overline{P}_{\text{fc}}\right) R_{0,\text{bat}}}}{2R_{0,\text{bat}}}, \tag{13}$$

which is then substituted into Eq. (5), so that the dynamic of the state can be calculated as shown in Eq. (14):

$$\dot{SoC} = -\frac{V_{\text{oc,bat}} - \sum_{i=1}^{3} V_i - \sqrt{\left(V_{\text{oc,bat}} - \sum_{i=1}^{3} V_i\right)^2 - 4\left(P_{\text{load}} - \overline{P}_{\text{fc}}\right) R_{0,\text{bat}}}}{2Q_{\text{bat}} R_{0,\text{bat}}}. \tag{14}$$

In Eq. (14), the resistance $R_{0,\text{bat}}$ and the open-circuit voltage $V_{\text{oc,bat}}$ are linked to the state SoC itself, as shown in Fig. 7a and b. In addition, as mentioned before, the derivations of changeable parameters V_1, V_2, V_3 with respect to SoC are defined to be zero, as shown in Eq. (15):

$$\frac{\partial V_1}{\partial SoC} = \frac{\partial V_2}{\partial SoC} = \frac{\partial V_3}{\partial SoC} = 0. \tag{15}$$

Because the fuel cell system power rate $\dot{P}_{\text{fc}}$ is defined as the control and P_{fc} is a changeable parameter, the derivation of $\overline{P}_{\text{fc}}$ with respect to the state variable also equals zero. Furthermore, the disturbance signal P_{load} does not depend on the SoC. As a result, the derivation of the SoC dynamic with respect to the state itself is displayed in Eq. (16):

$$\frac{\partial \dot{SoC}}{\partial SoC} = \left(\frac{\partial \dot{SoC}}{\partial V_{\text{oc,bat}}} \cdot \frac{\partial V_{\text{oc,bat}}}{\partial SoC} + \frac{\partial \dot{SoC}}{\partial R_{0,\text{bat}}} \cdot \frac{\partial R_{0,\text{bat}}}{\partial SoC}\right). \tag{16}$$

By substituting Eq. (16) into Eq. (10), the change rate of the costate is determined in Eq. (17):

$$\dot{\lambda}\left(t\right) = -\lambda\left(\frac{\partial \dot{SoC}}{\partial V_{\text{oc,bat}}} \cdot \frac{\partial V_{\text{oc,bat}}}{\partial SoC} + \frac{\partial \dot{SoC}}{\partial R_{0,\text{bat}}} \cdot \frac{\partial R_{0,\text{bat}}}{\partial SoC}\right). \tag{17}$$

With the help of Eq. (12) and Eq. (14), the partial derivative of the SoC dynamic with respect to the $V_{\text{oc,bat}}$ is calculated in Eq. (18):

$$\frac{\partial \dot{SoC}}{\partial V_{\text{oc,bat}}} = -\frac{1}{2Q_{\text{bat}} R_{0,\text{bat}}}\left(1 - \frac{V_{\text{diff,bat}}}{\sqrt{V_{\text{diff,bat}}^2 - 4\left(P_{\text{load}} - \overline{P}_{\text{fc}}\right) R_{0,\text{bat}}}}\right), \tag{18}$$

and the derivation of the state dynamic with respect to the battery resistance $R_{0,\text{bat}}$ results in Eq. (19):

$$\frac{\partial \dot{SoC}}{\partial R_{0,\text{bat}}} = \frac{1}{2Q_{\text{bat}} R_{0,\text{bat}}^2}\left(\frac{2 \cdot \left(P_{\text{load}} - \overline{P}_{\text{fc}}\right) R_{0,\text{bat}} - V_{\text{diff,bat}}^2}{\sqrt{V_{\text{diff,bat}}^2 - 4 \cdot \left(P_{\text{load}} - \overline{P}_{\text{fc}}\right) R_{0,\text{bat}}}} + V_{\text{diff,bat}}\right). \tag{19}$$

The other two terms in Eq. (17), the derivatives $\frac{\partial R_{0,\text{bat}}}{\partial SoC}$ and $\frac{\partial V_{\text{oc,bat}}}{\partial SoC}$ are obtained from the specific curves of batteries, as displayed in Fig. 8. After all these equations are prepared, it is possible to update the costate with Eq. (17).

In the application of the offline PMP, the initial and end SoC values are assumed to be 0.5, and the changeable parameters are initialized with zero. Because of the nonlinear split boundary value problem fronted with the offline PMP, only numeric solutions are possible. For that reason, the shooting method is applied to search for the correct starting costate value. Within each instant, the optimal control variable is chosen to minimize the Hamiltonian defined in Eq. (20):

$$\dot{P}_{\text{fc}}^{*}\left(t\right) = \underset{\dot{P}_{\text{fc}}(t)}{\text{argmin}} H\left(SoC, \dot{P}_{\text{fc}}, \Delta t, P_{\text{fc}}, \lambda, t\right). \tag{20}$$

As the starting values of the state, costate variable, the fuel cell system power and three parasitic voltages are defined, they can be updated in each time instant with Eqs. (2), (7), (8), (9), (14), and (17). As a result, the optimal sequence of various variables under the driving cycle can be found. Detailed information about the theory of optimal control can be found in [34].

In the next section, the two-dimensional dynamic programming will be introduced, emphasizing the algorithm's parallelization based on soft constraints to initialize the cost function.

4. Forward dynamic programming

4.1. Basics of optimal control

The problem of the optimal control can be summarized with the following features: fixed time interval, given initial and final states, multi-control multi-state, definite range and intervals of state and control variables, pre-known disturbance signals [35]. They are defined as follows:

$$\text{Cost functional} \quad J = h(\boldsymbol{x}(t_0)) + \int_{t_0}^{t_f} g(\boldsymbol{x}(t), \boldsymbol{u}(t), t)dt, \tag{21}$$

$$\text{Optimal control} \quad \boldsymbol{u}^{*}\left(t\right) = \underset{\boldsymbol{u}(t)}{\text{argmin}} J\left(\boldsymbol{x}_0, \boldsymbol{u}\left(t\right)\right), \tag{22}$$

$$\text{Dynamics of the system} \quad \dot{\boldsymbol{x}}(t) = \boldsymbol{f}(\boldsymbol{x}(t), \boldsymbol{u}(t), t), \tag{23}$$

$$\text{Boundary values} \quad \boldsymbol{x}\left(t_0\right) = \boldsymbol{x}_0 \quad \boldsymbol{x}\left(t_f\right) = \boldsymbol{x}_f, \tag{24}$$

$$\text{Range of control variables} \quad \boldsymbol{u}(t) \in \mathscr{U}(t) \subset \mathbb{R}^n, \tag{25}$$

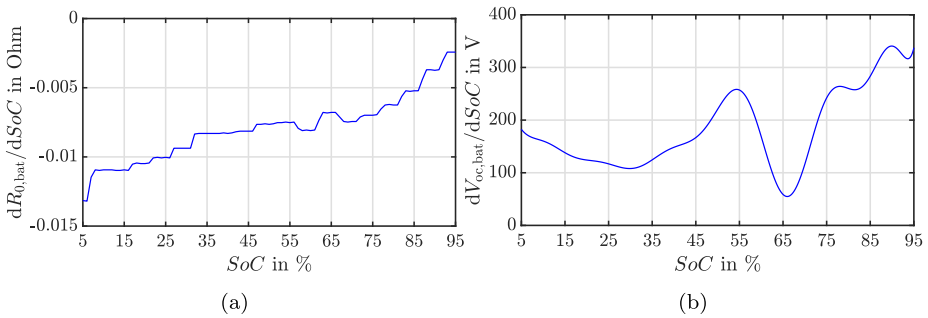

Fig. 8. Derivatives of the inner resistance $R_{0,\mathrm{bat}}$ and the open-circuit voltage $V_{\mathrm{oc,bat}}$ with respect to SoC: (a) $\frac{\partial R_{0,\mathrm{bat}}}{\partial SoC}$, (b) $\frac{\partial V_{\mathrm{oc,bat}}}{\partial SoC}$.

$$\text{Range of state variables} \quad \boldsymbol{x}(t) \in \mathscr{X}(t) \subset \mathbb{R}^m, \tag{26}$$

whereby t_0 and t_f are the start and end time, respectively, $h(\boldsymbol{x}(t_0))$ indicates the initial cost at t_0, $g(\boldsymbol{x}(t), \boldsymbol{u}(t), t)$ is the transient cost during each time interval, which depends on the actual time and the control and state variables at that instant. Moreover, the number of state and control variables are represented by n and m, respectively. It has to be mentioned that the range of the control variables in Eq. (25) suffers from both dynamic and static limits.

4.2. Principle of forward dynamic programming

Dynamic programming is only adaptable to discrete problems. Thus, a discretization of the continuous model is required. In the forward dynamic programming, each state can be formulated as a function of the state and control variables at the next time interval, as shown in Eq. (27):

$$\boldsymbol{x}[k-1] = \boldsymbol{F}(\boldsymbol{x}[k], \boldsymbol{u}[k], k), \quad k = 1, 2, \ldots, N, \tag{27}$$

whereby N represents the number of discretized time intervals and k the index of the time point. For a given set of control variables $\pi = \{\boldsymbol{u}[1], \boldsymbol{u}[2], \ldots, \boldsymbol{u}[N]\}$ and an initial state $\boldsymbol{x}[0]$, the cost functional with discretization can be determined in Eq. (28):

$$J_\pi(\boldsymbol{x}[N]) = h\left(\boldsymbol{x}[0]\right) + \sum_{k=1}^{N} g\left(\boldsymbol{x}[k], \boldsymbol{u}[k], k\right)\Delta t, \tag{28}$$

where $h(\boldsymbol{x}[0])$ is the initial cost and $g(\boldsymbol{x}[k], \boldsymbol{u}[k], k)\Delta t$ the transition cost. The optimal control sequence minimizes the cost function with expected end states $\boldsymbol{x}[N]$ in Eq. (29):

$$J^*\left(\boldsymbol{x}\left[N\right]\right) = \min_{\pi \in \Pi} J_\pi\left(\boldsymbol{x}\left[N\right]\right), \tag{29}$$

whereby Π represents the set of the accessible range of the control variables.

At each time stage k, the cost-to-go functions $J^*(\boldsymbol{x}[k])$ of all possible state variables are calculated. The iterative calculation moves forward in time domain step by step:

- Cost for the starting time point in Eq. (29)

$$J^*(\boldsymbol{x}[0]) = h(\boldsymbol{x}[0]). \tag{30}$$

- Iterative calculation based on the Bellman's principle of optimality, as shown in Eq. (31), for $k = 1$ to N:

$$J^*\left(\boldsymbol{x}\left[k\right]\right) = \min_{\boldsymbol{u}[k] \in \mathscr{U}[k]} \left(J^*\left(\boldsymbol{x}\left[k-1\right]\right) + g\left(\boldsymbol{x}[k], \boldsymbol{u}[k], k\right)\Delta t\right), \tag{31}$$

whereby $\boldsymbol{x}[k-1]$ is determined by using Eq. (27). After the forward calculation is finished, the optimal policy is found. Finally, we trace back from the final stage to determine the control and state variables' trajectories corresponding to the values of the final state.

The computational effort of dynamic programming implemented with embedded loops is exponential to the numbers of state and control variables, as shown in Eq. (32):

$$\mathscr{O}(N \cdot p^n \cdot q^m), \tag{32}$$

where q and p represent the discretization degree for the control and state variables, respectively, and N, m, n are the numbers of time stages, control, and state variables [34].

The next subsection will introduce the two-dimensional implementation of dynamic programming, with its advantages against implementing dynamic programming under the one-dimensional framework.

4.3. Two-dimensional dynamic programming to solve energy management

The one-dimensional dynamic programming in energy management has a significant drawback: it cannot deal with dynamic constraints on fuel cell systems precisely without side effects. Under the one-dimensional framework, a limitation of the fuel cell system power's change makes the fuel cell power at each instant depend on its value in the past. Therefore, the precondition of dynamic programming is violated, according to which the control variable and cost function should be independent of history. Therefore, the two-dimensional dynamic programming is introduced, as described in [23]. In this way, both the SoC and the fuel cell system power are defined as state variables, while the dynamic of fuel cell system power is chosen to be the control variable. In order to discretize the optimal control problem, the dynamics of state and control variable are defined as follows:

- State vector $\boldsymbol{x} = [x_1, x_2] = [SoC, P_\mathrm{fc}]$
- Control input $u = \frac{dP_\mathrm{fc}}{dt}$
- Difference equation regarding SoC is derived based on Eq. (14) and results in Eq. (33):

$$x_1\left[k-1\right] = x_1\left[k\right] + \Delta t \cdot \frac{I_\mathrm{bat}[k]}{Q_\mathrm{bat}}, \tag{33}$$

whereby the battery current $I_\mathrm{bat}[k]$ is reformulated in Eq. (34) from Eq. (13):

$$I_\mathrm{bat}\left[k\right] = \frac{V_\mathrm{diff,bat}\left[k\right]}{2R_\mathrm{0,bat}\left[k\right]} - \sqrt{\left(\frac{V_\mathrm{diff,bat}\left[k\right]}{2R_\mathrm{0,bat}\left[k\right]}\right)^2 - \frac{P_\mathrm{load}[k] - x_2[k]}{R_\mathrm{0,bat}\left[k\right]}}, \tag{34}$$

- Difference equation regarding the fuel cell system power in Eq. (35):

$$x_2[k-1] = x_2[k] - \Delta t \cdot u[k], \tag{35}$$

- Difference equations regarding the parasitic voltages are derived based on Eqs. (7)–(9) and they result in Eqs. (36)–(38):

$$V_1\left[k-1\right] = V_1\left[k\right] - \left(\frac{I_{\text{bat}}[k]}{C_1[k]} - \frac{V_1[k]}{C_1[k]\cdot R_1[k]},\right)\cdot\Delta t, \tag{36}$$

$$V_2\left[k-1\right] = V_2\left[k\right] - \left(\frac{I_{\text{bat}}[k]}{C_2[k]} - \frac{V_2[k]}{C_2[k]\cdot R_2[k]},\right)\cdot\Delta t, \tag{37}$$

$$V_3\left[k-1\right] = V_3\left[k\right] - \left(\frac{I_{\text{bat}}[k]}{C_3[k]} - \frac{V_3[k]}{C_3[k]\cdot R_3[k]},\right)\cdot\Delta t, \tag{38}$$

  Same as the PMP-based strategy, the parasitic voltages are described as changeable parameters dependent on time-state points.
- State constraints in Eq. (39):

$$\begin{array}{ll} 0.2\leqslant & x_1[k]\leqslant 0.9, \\ 0\text{kW}\leqslant & x_2[k]\leqslant 200\text{kW}, \end{array} \tag{39}$$

  where 200 kW is the maximal output power of the fuel cell system.
- Control constraint in Eq. (40):

$$-30\text{kW/s}\leqslant u[k]\leqslant 30\text{kW/s}, \tag{40}$$

  whereby the limits are assumed to be constant to reduce the complexity of the modeling. The reason is that this work mainly focuses on the algorithm instead of giving an accessible range of dynamic based on actual operational conditions. However, it is also possible to set them more appropriately according to the fuel cell system's actual states.
- Battery current limits in Eq. (41):

$$-900\text{A}\leqslant I_{\text{bat}}[k]\leqslant 900\text{A}. \tag{41}$$

The cost functional is formulated in Eq. (42):

$$J = \underbrace{h(x_1[0])}_{\text{initialization}} + \underbrace{\Delta t\sum_{k=1}^{N}\dot{m}_{\text{H}_2}(x_2[k])}_{\text{hydrogen}} + \underbrace{\mu\left(\sum_{k=1}^{N}\left|\text{Sign}\left(x_2\left[k\right]\right) - \text{Sign}\left(x_2\left[k+1\right]\right)\right|\right)}_{\text{switching on/off penalty}} + \underbrace{\Delta t\sum_{k=1}^{N}\sigma\cdot u[k]^2}_{\text{power dynamic penalty}} \tag{42}$$

where $h(x_1[0])$ represents the initialization based on SoC that enables the charge sustaining in the forward dynamic programming, μ is a penalty coefficient that reduces the frequency of the on/off operation of the fuel cell system, and σ penalizes the fuel cell system power dynamic.

In order to reduce the computational time under the two-dimensional implementation of dynamic programming, the parallelization of the algorithm will be introduced in the next subsection.

4.4. Parallel implementation

The matrix-based calculation in MATLAB enables the execution of all operations in one time step, which results in computational time in the order of $\mathcal{O}(N)$. During the forward calculation, the transition of states from the k-th time point to the $(k-1)$-th time point with various discretized control values are shown in Fig. 9. These control inputs result in three possible situations:

1. The new state in the $(k-1)$-th time point locates just in the discrete states, as Point A shows.
2. The new state in the $(k-1)$-th time point locates between the discrete states, as Point B shows.
3. The new state in the $(k-1)$-th time lies outside of the permitted range of the states, as Point C shows.

For the second situation, the cost-to-go values of the resulted state $J^*(\boldsymbol{x}[k-1])$ are estimated using linear interpolation. For situation C, the control input corresponds to this invalid transition will not be chosen. After that, the cost-to-go values in the k-th time stage can be determined with Eq. (31). Similarly, for states in the new stage that locate outside the accessible range under all discrete control values, their current cost-to-go function is added with a vast value to avoid a trajectory through these states.

In the next subsection, the semi-physical mechanism to initialize the cost function will be introduced.

4.5. Soft constraints

According to Eq. (30), before the iterative calculation starts, the initial cost-to-go function corresponding to each discrete state at the first time stage should be determined. As the transition of states between time stages is not point-to-point, a soft constraints mechanism is required. It has to ensure that the SoC trajectory under forward dynamic programming begins with a value close enough to the given initial SoC. Regarding the soft constraints, if the penalty for the initial SoC values, that are not equal to the given one, is too small, the resulting optimal SoC trajectory will not start with the expected initial value. Conversely, if the penalty becomes too strong, the cost-to-go values lose their physical meaning, since interpolation is used to estimate cost-to-go values. Then, a substantial penalty can cause deviation of cost-to-go values from the cost function. This difficulty is the reason that most literature adopts point-to-point transition patterns. In this work, a semi-physical approach is used in the design of soft constraints. The state matrix in the first time stage is divided into two parts. All states with SoC values in a range from $\text{SoC}_{\text{initial}} - \Delta\text{SoC}$ to $\text{SoC}_{\text{initial}} + \Delta\text{SoC}$ belong to the "narrow" part, while ΔSoC represents the discretization degree of the state variable SoC. The remaining states belong to the "rest" part. With the help of the derivative of the fuel cell specific consumption curve, as displayed in Fig. 10, the initial cost corresponding to each state location is determined as follows: The initial states, that lie in part "narrow" and have a lower SoC than the expected initial value, are assigned a negative value of the consumed hydrogen, which is needed to be charged from the expected initial SoC to the current SoC values. Thereby, the minimal derivative specific consumption is utilized, which corresponds to 10% of the maximal fuel cell system power. Conversely, the states of part "narrow", which have higher SoC than the desired initial value, are assigned the value of the consumed hydrogen, which is required to be charged from the current SoC to the expected initial SoC. In this case, the maximal derivative specific consumption value is used, which has a fuel cell system power of 200 kW net. For the remaining states outside of the part "narrow", the consumed hydrogen mass is determined by using a linearly extrapolated value for the derivative specific consumption

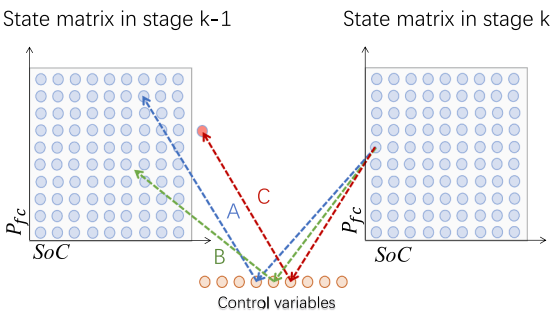

Fig. 9. Transition pattern of the parallelized algorithm.

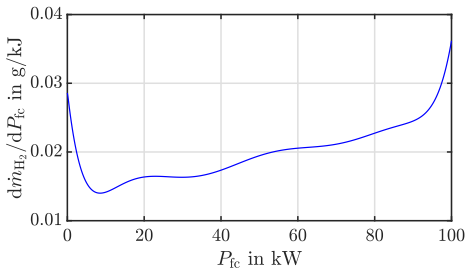

Fig. 10. Derivative of specific consumption with respect to the output fuel cell system power.

depending on the difference between the current SoC values and the expected initial value. In this way, it is ensured that the SoC trajectory begins with the desired value. Furthermore, the cost-to-go function keeps its physical meanings, as the initial cost within the part "narrow" is defined by using the specific curves of the fuel cell system.

The next subsection will introduce the mechanism to update the parasite voltages, which are considered in dynamic programming.

4.6. Update of the parasitic voltages

In the offline DP-based strategy, the parasitic voltages are also implemented to reach higher accuracy. According to Eqs. (36)–(38), the parasitic voltages in the $(k-1)$-th time point are dependent on the battery current and parasitic voltages of the k-th time point. As shown in Eq. (34), the battery current $I_{bat}[k]$ is also determined with parasitic voltages $V_1[k]$, $V_2[k]$, and $V_3[k]$ of the same time point. However, the parasitic voltages at the current time point are unknown. As a solution to this problem, an algorithm is implemented, as shown in Fig. 11a. This algorithm is summarized as follows:

- Step 1: The battery current is calculated temporarily without parasitic voltages with Eq. (43):

$$I_{bat}\left[k\right] = \frac{V_{oc,bat}\left[k\right]}{2R_{0,bat}\left[k\right]} - \sqrt{\left(\frac{V_{oc,bat}\left[k\right]}{2R_{0,bat}\left[k\right]}\right)^2 - \frac{P_{load}[k] - x_2[k]}{R_{0,bat}\left[k\right]}}, \tag{43}$$

  whereby the open-circuit voltage $V_{oc,bat}[k]$ replaces the difference voltage $V_{diff,bat}[k]$.
- Step 2: The SoC and the fuel cell system power in the $(k-1)$-th time point are estimated for the first time by using Eq. (33) and Eq. (35). Then, the parasitic voltages in the $(k-1)$-th time point are interpolated for the first time based on the estimated SoC and the fuel cell system power.
- Step 3: The estimated parasitic voltage combinations corresponding to different control variables are assumed to be the same in the k-th time point.
- Step 4: Return to the first step, and the battery current $I_{bat}[k]$ can be for the second time determined by using Eq. (34), with the parasitic voltages resulted in the third step.
- Step 5: The SoC and fuel cell system power are calculated for the second time by using Eq. (33) and Eq. (35), the parasitic voltage in the $(k-1)$-th time point are also interpolated for the second time.

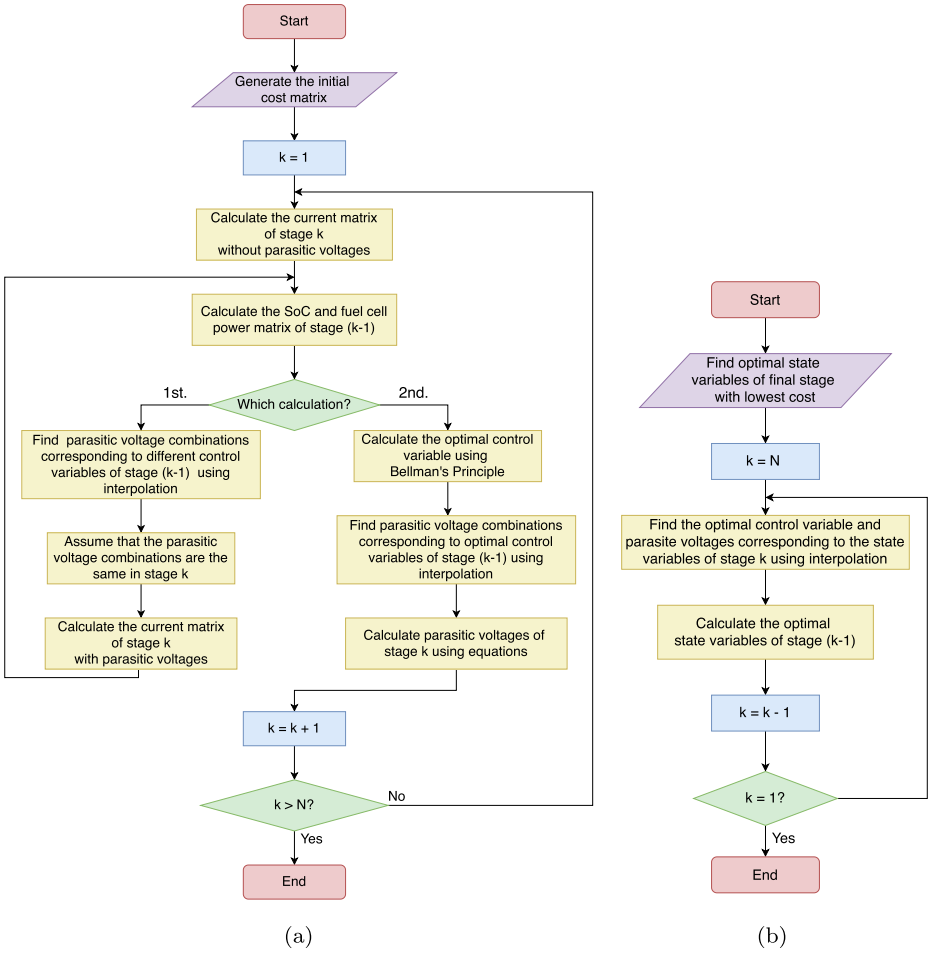

Fig. 11. (a) Forward dynamic programming, (b) Traceback.

- Step 6: The control variable in the k-th time point is determined according to the Bellman's principle of optimality, as shown in Eq. (31).
- Step 7: The parasitic voltages in the k-th time point are updated by using Eqs. (36)–(38) in a reverse way.

After the forward iteration, the optimal control policy is determined. Finally, the desired trajectory of SoC, fuel cell system power and parasitic voltages are found by using a traceback, which is displayed in Fig. 11b. The pseudo-code of the entire algorithm can be found in the appendix.

In the next section, the correctness of the PMP and dynamic programming are validated, and a comparison based on their results will be given.

5. Offline results

As mentioned before, the entire load power trajectory is the input for the offline strategies as the disturbance signal. Through a forward calculation in Simulink, the load power trajectory is calculated, as shown in Fig. 12. Thereby, the velocity profile is displayed together, and high positive power peaks occur during acceleration phases, while negative ones can be observed during regenerative braking. The discretization of dynamic programming is summarized in Table 1.

The resulting trajectories regarding various variables are displayed in Fig. 13. The SoC trajectories almost overlap, as shown in Fig. 13b, which correspond to the battery current trajectories in Fig. 13a. It is noticeable that the SoC trajectories, during the meantime, display more deviation from each other compared to the remaining time. The reason lies in the sparse time discretization in dynamic programming compared to 0.05 s in PMP. For the same reason, the fuel cell system power trajectories in Fig. 13c, resulting from dynamic programming, show much more oscillation compared to that from the PMP-based strategy. However, the fuel cell system power trajectory from the PMP-based strategy lies in the average part of the trajectory from dynamic programming, which proves the correctness of both methods.

The parameters related to the fuel economy are summarized in Table 2. The hydrogen consumption is 16096 g and 15856.8 g for dynamic programming and PMP, respectively, with a difference of 1.5%. The reason lies in the comparably sparse discretization in the time domain for dynamic programming. The average load power in dynamic programming is 111.9 kW, compared to 110.4 kW in PMP, and a difference of about 1.4% from each other exists. As mentioned before, the most significant difference is considering the parasite R-C branches of batteries in the offline calculation, and here, the various voltages can be found in Fig. 13d, e, and f. The high degree of overlapping in the trajectories validates the effectiveness of both methods again.

From the results above, it may be misleading that the PMP-based strategy can overtake dynamic programming regarding the accuracy of results and less computational time. However, as mentioned in the first introduction part, the constraints on the state variable can not be well handled by the PMP-based strategy, which, however, belongs to the

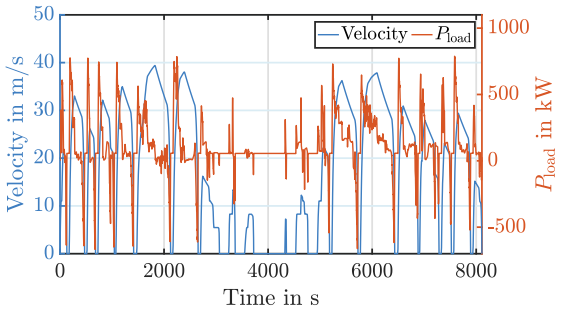

Fig. 12. Trajectories of load power and velocity.

Table 1
Setup of discretization degree during implementation of dynamic programming.

Parameter	Minimum	Maximum	Step	Stage number
Time [s]	0	8110	1	8111
P_{fc} [kW]	0	200	5	41
SoC	0.2	0.9	0.0001	7001
$\frac{dP_{fc}}{dt}$ [kW/s]	−30	30	5	13

advantage of dynamic programming. As an example, the SoC limits are changed to be 0.45 for minimum and 0.65 for maximum. The results can be found in Fig. 14, whereby Fig. 14a displays the fuel cell power trajectories and Fig. 14b the SoC trajectories. In order to maintain the SoC within the new limits, the fuel cell power is reduced during the early period and increased during the later period. As the cost to maintain the SoC within a narrower range, the hydrogen consumption increases from 16096 g to 16100 g.

Another advantage of the PMP-based strategy with the fuel cell system power rate as the control variable lies in being able to easily modifying the cost function to penalize the fuel cell power dynamic with a weighting factor σ, as follows:

$$H\left(SoC,\dot{P}_{fc},\Delta t,P_{fc},\lambda,t\right)=\dot{m}_{H_2}\left(P_{fc}\left(t\right)+\frac{1}{2}\cdot\dot{P}_{fc}\cdot\Delta t\right)+\lambda\left(t\right)\cdot\dot{SoC}\left(t\right)+\sigma\dot{P}_{fc}^{2}. \tag{44}$$

In order to analyze the effects of the damping factor on the hydrogen consumption and the power dynamic of the fuel cell system, the offline PMP is executed with different damping factors. The hydrogen consumption under different damping factors σ is collected in Table 3. With the damping factor raised, the hydrogen consumption increases by a maximum of 3.5 g, as shown in Fig. 15. However, the power dynamic is significantly reduced, and the power trajectory becomes smoother, as shown in Fig. 16.

In the next section, the offline strategy is used to evaluate a rule-based strategy's fuel economy based on measurement on the test bench.

6. Experimental validation

The configuration of the whole test bench to validate various strategies is displayed in Fig. 17. There are three dc/dc converters, one for the fuel cell system to control the output fuel cell system power actively, one for the traction side, which is controlled to maintain the dc-link voltage at 1650 V, the remaining one for the load side, which is implemented as power control. Instead of a real driveline consisting of inverters, motors, gear, tires, and the whole train, the load power is emulated by using the load side converter. Thereby, the power demand is simulated in dSPACE SCALEXIO and then implemented by the load side dc/dc converter. It is worth mentioning that the whole test bench is symmetrical, where the traction and the load battery systems are the same, which provide high peak power, and the load unit is also actively controlled to absorb the average fuel cell system power. The load unit can be used to adjust the initial SoC of both batteries before simulating driving cycles.

Initially, the rated charge and discharge currents of the battery system are 900 A, the maximal power of the fuel cell system, and the load unit is 200 kW. In this case, the high peak power of about 900 kW in Fig. 12 can be emulated without over current problems for batteries. Due to technical limitations of the test objects, the system's power is restricted. There are two main consequences for test bench operation. On the one side, a shortened driving cycle in Fig. 18 is used due to the limited capacity of the load battery, considering its SoC limits. On the other side, the load power implemented by the load side dc/dc converter must be reduced, because the load battery system alone can not cover that maximal power. As the battery system consists of three parallel branches, each of which can be separately switched off by software, the

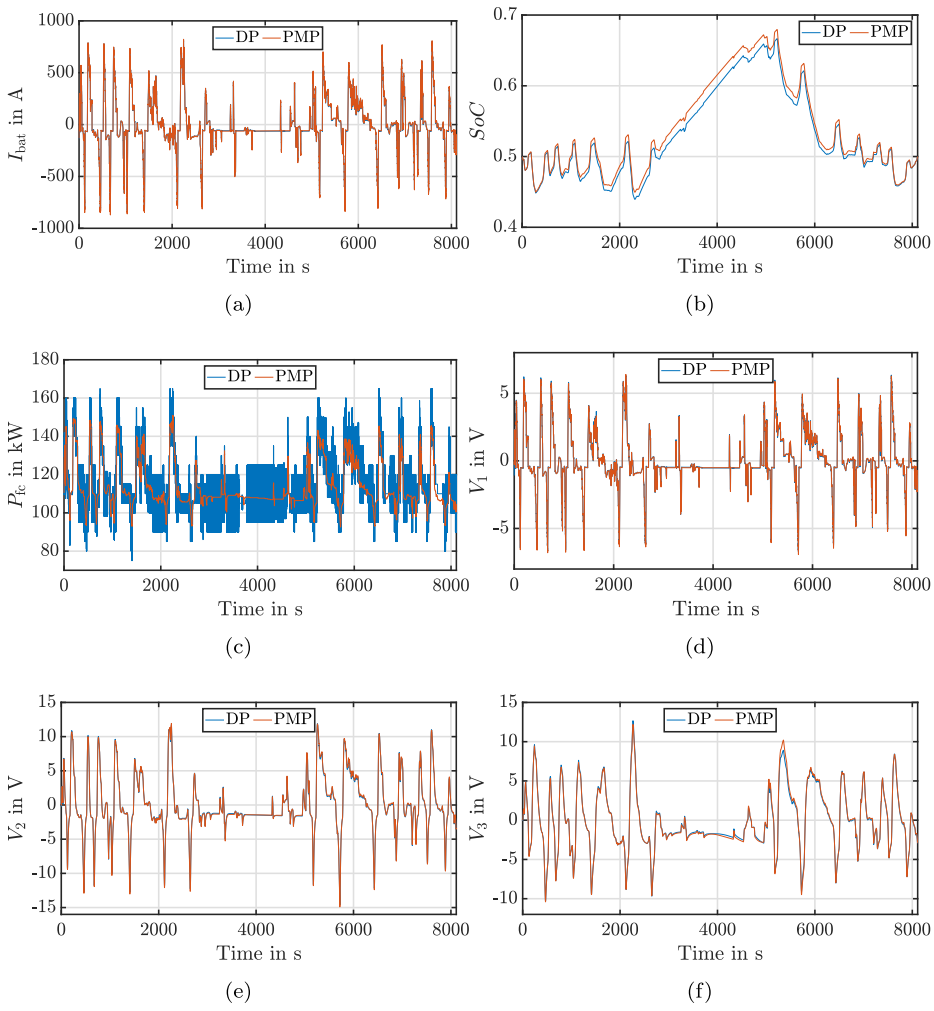

Fig. 13. Results of the PMP-based strategy and dynamic programming: (a) Battery current trajectories, (b) SoC trajectories, (c) Fuel cell system power trajectories, (d) V_1 trajectories, (e) V_2 trajectories, (f) V_3 trajectories.

Table 2
Comparison between dynamic programming and PMP.

Parameter	Dynamic programming	PMP	Difference
Time step [s]	1	0.05	–
$\overline{P}_{fc}$ [kW]	111.9	110.4	1.4%
m_{H_2} [g]	16096	15856.8	1.5%

load power is reduced to be 2/3 of the original value. Moreover, the fuel cell system power should not be downscaled to ensure that the validation of energy management strategies regarding fuel economy remains meaningful. Therefore, the load power to be implemented with the help of the load side dc/dc converter is formulated, as shown in Eq. (45):

$$P_{\text{load,testbench}} = \frac{2}{3}\cdot P_{\text{load}} + \frac{1}{3}\cdot P_{\text{fc}}. \tag{45}$$

Then, the battery power in the test bench can be theoretically calculated, as shown in Eq. (46):

$$P_{\text{bat,testbench}} = P_{\text{load,testbench}} - P_{\text{fc}} = \frac{2}{3}\cdot\left(P_{\text{load}} - P_{\text{fc}}\right). \tag{46}$$

Because only two branches of the traction battery system are used, the

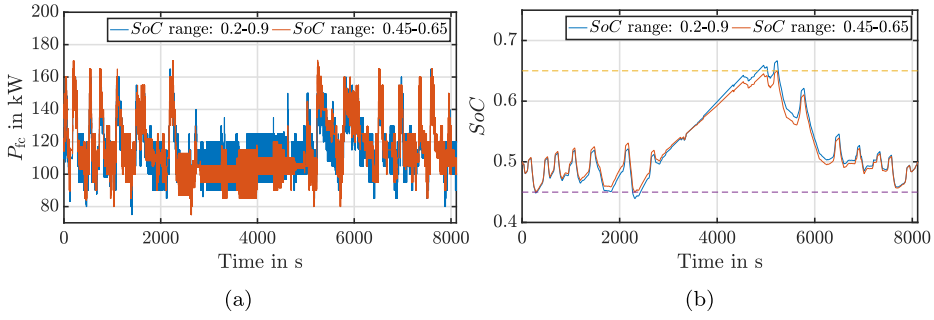

Fig. 14. Resulted trajectories of dynamic programming under difference SoC limits: (a) Fuel cell system power, (b) SoC.

Table 3
Influence of the penalty factor σ on hydrogen consumption.

Factor σ [10^{-6}]	Hydrogen consumption [g]
0	15856.8
0.25	15856.9
0.5	15857.9
0.75	15859.0
1	15860.3

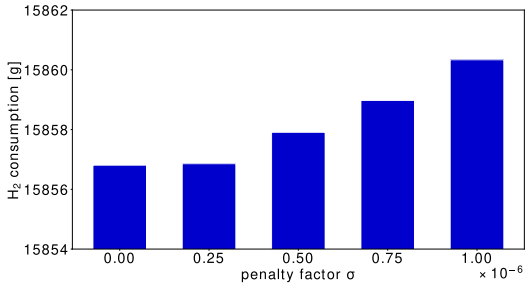

Fig. 15. Hydrogen consumption dependent on the damping factor σ.

SoC trajectory in praxis can reflect the simulated SoC trajectories to a large degree, except for the non-linearity in the power loss of the dc/dc converter due to scaling. A comparison between the simulated model and the test bench is summarized in Table 4.

The offline strategies are used to validate the real-time strategies. Here, a rule-based strategy as shown in Fig. 19 is to be validated. Thereby, the fuel cell system power is maintained at the average sum of the load power and the battery loss as long as the SoC lies within given limits. In the case of overcharging, the fuel cell system power is reduced by a factor of b. Oppositely, the fuel cell system power is increased by another factor compared to the average value in the case of over-discharging.

The measured power distribution and the various trajectories under the rule-based strategy are displayed in Fig. 20. The fuel cell power changes in steps according to the rule-based strategy, as shown in Fig. 20c. Due to the limited implementable power ramp through power electronics, a small delay between the actual and the reference velocity profiles can be found in Fig. 20f. The simulated SoC and terminal battery voltages are also added in the Fig. 20a and b to the measured ones, and overlapping is observed. Based on that, the modeling of battery systems is validated. Moreover, the measured SoC end value is 0.51, and the simulated one is 0.513. The correctness of modeling the specific consumption curve of the fuel cell system is validated through a comparison

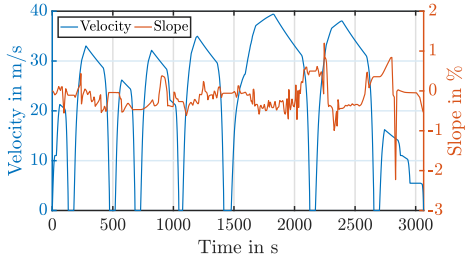

Fig. 18. The shortened driving cycle for measurement on test bench.

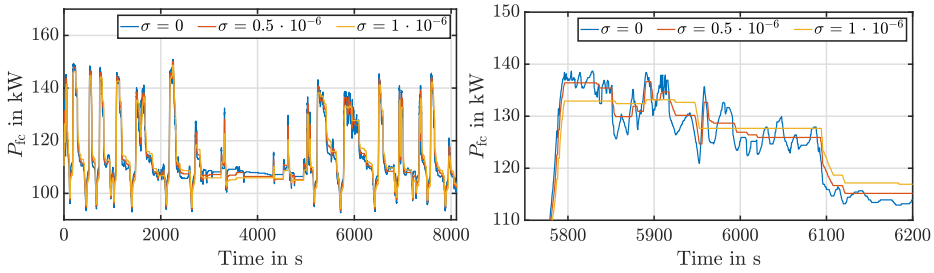

Fig. 16. Fuel cell system power trajectories resulted from the offline PMP under different damping factors: (a) Without enlargement, (b) With enlargement.

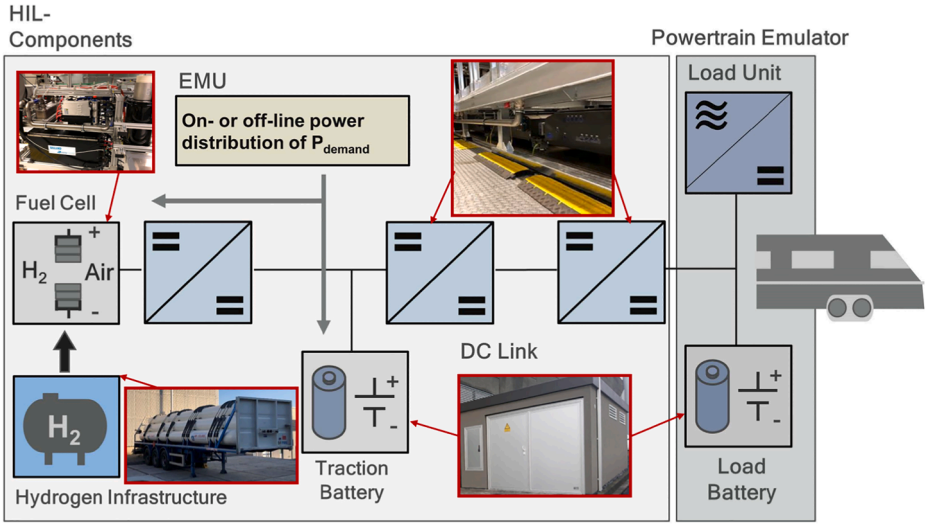

Fig. 17. Configuration of test bench with load power emulated at the Institute for Combustion Engines (VKA).

Table 4
Comparison between the simulated model and the test bench.

Parameters	Simulation	Test bench
Number of battery branches	3	2
Maximal load power	900 kW	600 kW
Minimal load power	−900 kW	−600 kW
Time of driving cycles	8110 s	3065 s

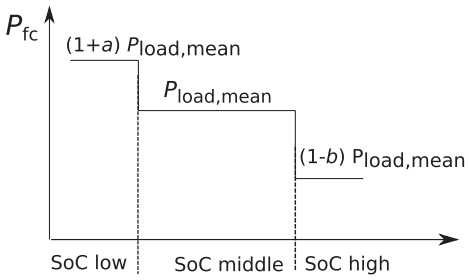

Fig. 19. Rule-based strategy, to be validated by comparison to off-line strategies.

between the simulated hydrogen consumption and the measured one in Fig. 20d. Thereby, a difference of 0.5% between the measured consumption of 5803 g and the simulated value of 5774 g for a distance of 70 km results. The fuel cell system power rate is limited to about ±5 kW/s through the internal control of the fuel cell system, as shown in Fig. 20c. Moreover, a negligible deviation of the actual fuel cell system power from its reference value can be found. In Fig. 20e, the power distribution under the rule-based strategy is displayed, whereby the fuel cell system covers the averaged load power, and the battery system provides the high peak power.

In order to evaluate the fuel economy of the rule-based strategy, the measured fuel cell and the battery power are summed, and the offline methods are used to determine the optimal fuel cell system power trajectories. The offline determined control sequence is then implemented in the test bench. The measured trajectories of fuel cell system power under offline strategies are displayed in Fig. 21a and the SoC in Fig. 21b. As a comparison, the offline calculated fuel cell system power and SoC trajectories, and the ones resulted from the rule-based strategy are also added. As for the fuel cell system power, during strong acceleration, the fuel cell system power under the optimal strategy is above its averaged value, while below its averaged value during regenerative braking. The offline calculated hydrogen consumption is 5718 g, about 1.5% less than that in the rule-based strategy, with almost the same SoC end value as that in the rule-based strategy. On the test bench, since the offline calculated fuel cell system power series cannot be fully implemented without delay and static deviations, the measured hydrogen consumption of 5644 g is a little different from the offline calculated value. Meanwhile, the measured SoC end value equals 0.5, 0.01 less than the SoC end value under the offline calculated strategy. The costate value

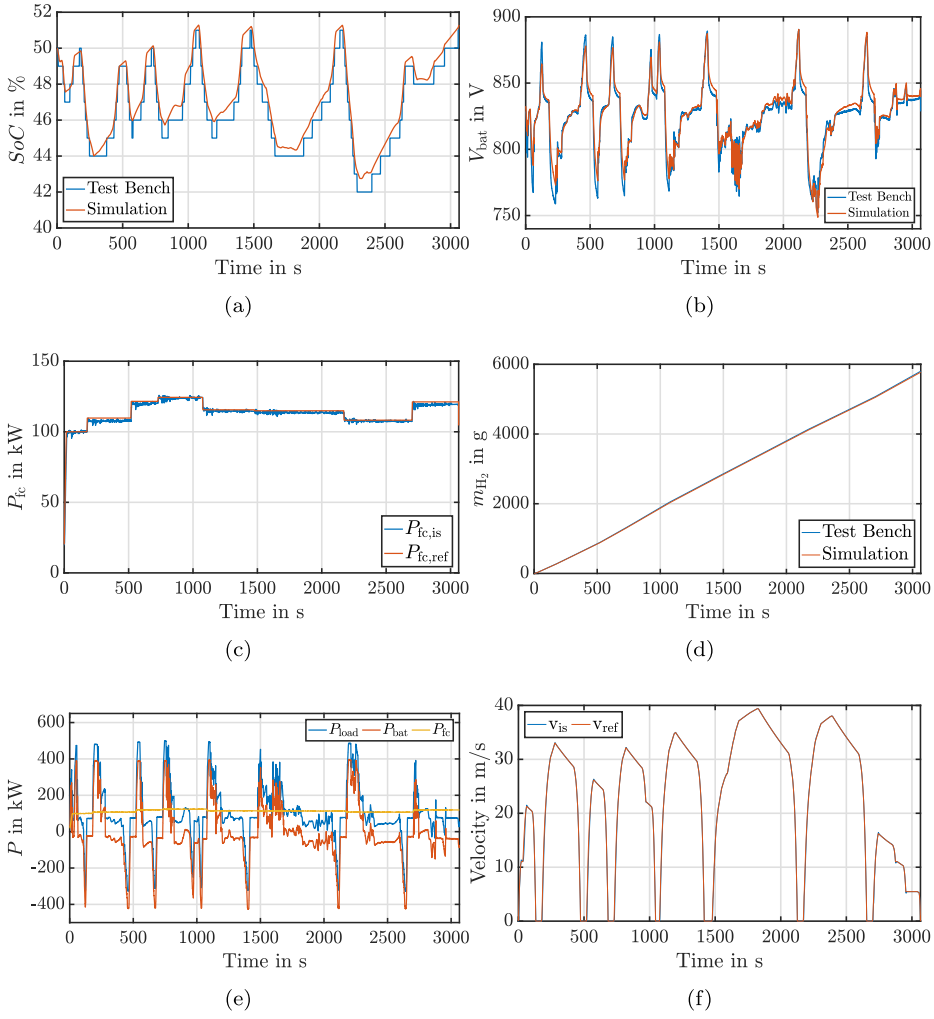

Fig. 20. Measured trajectories under the rule-based strategy: (a) SoC, (b) Battery voltage, (c) Fuel cell system power, (d) Hydrogen consumption, (e) Measured power distribution, (f) Velocity profiles.

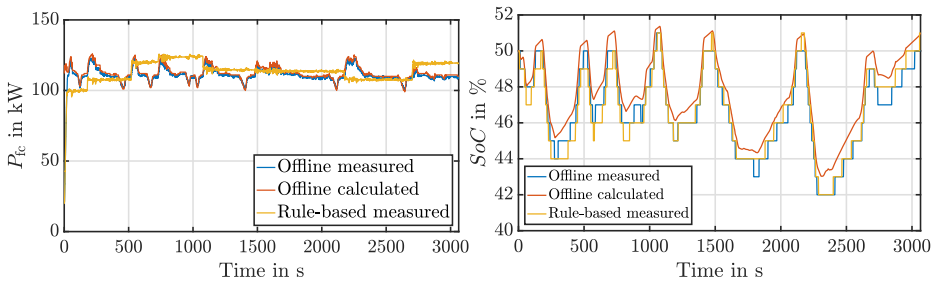

Fig. 21. Measured and calculated results of offline PMP strategy and measured results of rule-based strategy: (a) Fuel cell system power, (b) SoC.

trajectory under the offline PMP strategy is shown in Fig. 22. Its average amplitude of 8251 g can be used to convert the 1% SoC to the corresponding hydrogen consumption. The adjusted hydrogen consumption is 5726.5 g, 0.15% different from the analytically determined value. So far, the benefits of the developed offline strategies with complicated battery models considered are observed, which enables the offline results to be regenerated on the test bench. In the future, for validation of other strategies, there will be no need to validate the offline results on the test bench anymore, because the offline calculated results are accurate enough to evaluate the effectiveness of other strategies. Summarily, a comparison between the rule-based strategy, the offline PMP, and the measured PMP on the test bench regarding hydrogen consumption with and without compensation of the difference in SoC end values is given in Table 5.

Table 5
Comparison among the rule-based strategy, the offline PMP, and the measured PMP.

Parameters	Rule-based	PMP	PMP measured
SoC_{end}	0.51	0.51	0.5
m_{H_2} [g]	5803	5718	5644
Diff. from PMP	+ 1.5%	–	–
$\bar{\lambda}$ for compensation [g]	–	8251	–
m_{H_2} after compensation [g]	–	–	5726.5
Diff. from PMP after compensation	–	–	+ 0.15%

7. Conclusions

Offline strategies based on PMP and dynamic programming are implemented in this work. By implementing various resistance and capacitor elements within the battery simulation model, the relaxation of the battery voltage has been considered. Therefore, transient loads could also be applied to the battery system sufficiently. Moreover, the fuel cell power rate is defined as the control variable instead of the fuel cell system power, which differs fundamentally from the reviewed literature. In this way, the power rate can be actively controlled instead of indirectly introducing a weighting factor to limit fuel cell power dynamics. The results of PMP and dynamic programming are validated by each other. Thereby, the hydrogen consumption resulted from dynamic programming is about 1.5% higher than that resulted from PMP because of the comparably sparse discretization in the time domain for dynamic programming. Furthermore, the calculation of dynamic programming is parallelized to utilize the hardware resources and to reduce computation time. Thereby, the mechanism of soft constraints is introduced to enable interpolation to estimate the cost-to-go values. As next, the influence of the damping factor on the oscillation of the fuel cell power and fuel economy is analyzed, and it is possible to reduce the power dynamic without the loss of fuel economy. At last, the accuracy of the results from offline strategies is validated through measurements on the test bench at the Center for Mobile Propulsion (CMP). The results of offline PMP are regenerated on the test bench, with a 0.15% difference in the hydrogen consumption between calculation and measurement. Due to their high accuracy, the implemented offline strategies provide more precise reference results to evaluate online strategies than as found in the literature. For future work, the adaptive Pontryagin's minimum principle-based strategy will be implemented to consider the parasitic voltages over the resistor–capacitor branches.

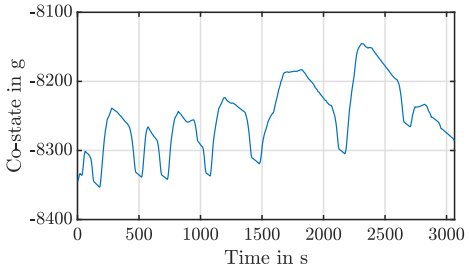

Fig. 22. Costate trajectory resulted from the offline PMP-based strategy.

CRediT authorship contribution statement

Hujun Peng: Conceptualization, Methodology, Formal analysis, Validation, Writing - original draft. **Zhu Chen:** Software, Data curation, Validation. **Jianxiang Li:** Software, Data curation, Validation. **Kai Deng:** Writing - review & editing. **Steffen Dirkes:** Writing - review & editing, Resources. **Cem Ünlübayir:** Writing - review & editing. **Andreas Thul:** Project administration, Writing - review & editing. **Lars Löwenstein:** Resources, Writing - review & editing. **Stefan Pischinger:** Funding acquisition, Resources. **Kay Hameyer:** Funding acquisition, Writing - review & editing.

Declaration of Competing Interest

The authors declare that they have no known competing financial interests or personal relationships that could have appeared to influence the work reported in this paper.

Appendix A. Pseudocode for parallelized two-dimensional dynamic programming

Algorithm 1. Forward Iteration of Dynamic Programming

Algorithm 1: Forward Iteration of Dynamic Programming

Initialize: $cost_{\text{init}}, SoC, P_{\text{fc}}, u$

/* Initialize the two-dimensional cost and state matrix and the control vector at the starting stage */

$cost_{\text{opt}} = cost_{\text{init}}$

for $k < n_t$ **do**

/* Iteration in all time stages */

$cost_{\text{saved}} = cost_{\text{opt}}$

/* Save the two-dimensional cost-to-go matrix of last time stage. */

$[SoC_{\text{prev}}, P_{\text{fc,prev}}] =$ transition(SoC, P_{fc}, u)

/* Calculate the three-dimensional state matrix of the previous stage without parasite voltages, constraints on states are considered. */

$[U_{1,\text{prev}}, U_{2,\text{prev}}, U_{2,\text{prev}}] =$ interpolation_U$(U_{1,\text{saved}}, U_{2,\text{saved}}, U_{2,\text{saved}}, SoC_{\text{prev}}, P_{\text{fc,prev}})$

/* Determine the three-dimensional matrix of previous parasite voltages with interpolation */

$U_1 = U_{1,\text{prev}}$

$U_2 = U_{2,\text{prev}}$

$U_3 = U_{3,\text{prev}}$

/* Assume that the current parasite voltages are same as the previous stage */

$[SoC_{\text{prev}}, P_{\text{fc,prev}}, I] =$ transition$(SoC, P_{\text{fc}}, u, U_1, U_2, U_3)$

/* Calculate three-dimensional state matrix of the previous stage again with parasite voltages */

$cost_{\text{prev}} =$ interpolation_Cost$(cost_{\text{opt}}, SoC_{\text{prev}}, P_{\text{fc,prev}})$

/* Determine the three-dimensional cost-to-go matrix of previous states with interpolation */

$cost_{\text{interval}} =$cal_cost$(P_{\text{fc}}, P_{\text{fc,prev}})$

/* Calculate the three-dimensional matrix of transition costs */

$cost_{\text{total}} = cost_{\text{prev}} + cost_{\text{interval}}$

$(cost_{\text{opt}}, u_{\text{opt}}) =$ find_min$(cost_{\text{total}})$

/* Find minimal cost and the corresponding control */

$SoC_{\text{prev,opt}} =$ find_optimal$(SoC_{\text{prev}}, u_{\text{opt}})$

$P_{\text{fc,prev,opt}} =$ find_optimal$(P_{\text{fc,prev}}, u_{\text{opt}})$

$I_{\text{opt}} =$ find_optimal(I, u_{opt})

/* Determine the states of previous stage and current corresponding to optimal controls */

$(U_{1,\text{prev,opt}}, U_{2,\text{prev,opt}}, U_{3,\text{prev,opt}}) =$ interpolation_U$(U_{1,\text{saved}}, U_{2,\text{saved}}, U_{3,\text{saved}}, SoC_{\text{prev,opt}}, P_{\text{fc,prev,opt}})$

/* Determine two-dimensional matrix of parasite voltages corresponding to optimal controls */

$(U_{1,\text{saved}}, U_{2,\text{saved}}, U_{3,\text{saved}}) =$ update_U$(U_{1,\text{prev,opt}}, U_{2,\text{prev,opt}}, U_{3,\text{prev,opt}}, I_{\text{opt}})$

/* Update parasite voltages of current stage and save in two-dimensional matrix */

Save$(P_{\text{fc,prev,opt}})$ /* save optimal trajectories */

$cost_{\text{end}} = cost_{\text{opt}}$

traceback

References

[1] World premiere: Alstom's hydrogen trains enter passenger service in lower saxony, https://www.alstom.com/press-releases-news/2018/9/world-premiere-alstoms-hydrogen-trains-enter-passenger-service-lower, accessed September 30; 2020.

[2] Brennstoffzellen: Siemens beauftragt ballard power, https://www.iwr.de/news.php?id=34729, accessed December 18; 2019.

[3] Karaki SH, Jabr R, Chedid R, Panik F. Optimal energy management of hybrid fuel cell electric vehicles. Tech rep, SAE Technical Paper; 2015.

[4] Li T, Liu H, Zhao D, Wang L. Design and analysis of a fuel cell supercapacitor hybrid construction vehicle. Int J Hydrogen Energy 2016;41(28):12307–19. https://doi.org/10.1016/j.ijhydene.2016.05.040.

[5] Sulaiman N, Hannan M, Mohamed A, Ker PJ, Majlan E, Daud WW. Optimization of energy management system for fuel-cell hybrid electric vehicles: Issues and recommendations. Appl Energy 2018;228:2061–79.

[6] Liu C, Wang Y, Wang L, Chen Z. Load-adaptive real-time energy management strategy for battery/ultracapacitor hybrid energy storage system using dynamic programming optimization. J Power Sources 2019;438:227024. https://doi.org/10.1016/j.jpowsour.2019.227024.

[7] Peng J, He H, Xiong R. Rule based energy management strategy for a series–parallel plug-in hybrid electric bus optimized by dynamic programming. Appl Energy 2017;185:1633–43.

[8] Zhao M, Shi J, Lin C. Optimization of integrated energy management for a dual-motor coaxial coupling propulsion electric city bus. Appl Energy 2019;243:21–34.

[9] Peng H, Li J, Thul A, Deng K. C. A scalable, causal, adaptive rule-based energy management for fuel cell hybrid railway vehicles learned from results of dynamic programming. eTransportation 2020:100057.

[10] Peng H, Li J, Löwenstein L, Hameyer K. A scalable, causal, adaptive energy management strategy based on optimal control theory for a fuel cell hybrid railway vehicle. Appl Energy 2020;267:114987.

[11] Xie S, Hu X, Xin Z, Brighton J. Pontryagin's minimum principle based model predictive control of energy management for a plug-in hybrid electric bus. Appl Energy 2019;236:893–905.

[12] Anselma PG, Biswas A, Belingardi G, Emadi A. Rapid assessment of the fuel economy capability of parallel and series-parallel hybrid electric vehicles. Appl Energy 2020;275:115319.

[13] Kandidayeni M, Macias A, Boulon L, Kelouwani S. Investigating the impact of ageing and thermal management of a fuel cell system on energy management strategies. Appl Energy 2020;274:115293.

[14] Li X, Wang Y, Yang D, Chen Z. Adaptive energy management strategy for fuel cell/battery hybrid vehicles using pontryagin's minimal principle. J Power Sources 2019;440:227105.

[15] Bellman R. The theory of dynamic programming, Tech. rep., Rand corp santa monica ca; 1954.

[16] Odeim F, Roes J, Heinzel A. Power management optimization of a fuel cell/battery/supercapacitor hybrid system for transit bus applications. IEEE Trans Veh Technol 2016;65(7):5783–8. https://doi.org/10.1109/TVT.2015.2456232.

[17] Kim N, Ha S, Jeong J, Cha SW. Sufficient conditions for optimal energy management strategies of fuel cell hybrid electric vehicles based on pontryagin's minimum principle. Proc Inst Mech Eng, Part D: J Automobile Eng 2016;230(2):202–14. https://doi.org/10.1177/0954407015583408.

[18] Catalão JPdS, Pousinho HMI, Mendes V. Scheduling of head-dependent cascaded reservoirs considering discharge ramping constraints and start/stop of units. Int J Electr Power Energy Syst 2010;32(8):904–10.

[19] Jafari M, Malekjamshidi Z. Optimal energy management of a residential-based hybrid renewable energy system using rule-based real-time control and 2d dynamic programming optimization method. Renew Energy 2020;146:254–66. https://doi.org/10.1016/j.renene.2019.06.123.

[20] Ansarey M, Shariat Panahi M, Ziarati H, Mahjoob M. Optimal energy management in a dual-storage fuel-cell hybrid vehicle using multi-dimensional dynamic programming. J Power Sources 2014;250:359–71. https://doi.org/10.1016/j.jpowsour.2013.10.145.

[21] Xu L, Mueller CD, Li J, Ouyang M, Hu Z. Multi-objective component sizing based on optimal energy management strategy of fuel cell electric vehicles. Appl Energy 2015;157:664–74. https://doi.org/10.1016/j.apenergy.2015.02.017.

[22] Jiang H, Xu L, Li J, Hu Z, Ouyang M. Energy management and component sizing for a fuel cell/battery/supercapacitor hybrid powertrain based on two-dimensional optimization algorithms. Energy 2019;177:386–96. https://doi.org/10.1016/j.energy.2019.04.110.

[23] Peng H, Li J, Deng K, Thul A, Li W, Löwenstein L, Sauer DU, Hameyer K. An efficient optimum energy management strategy using parallel dynamic programming for a hybrid train powered by fuel-cells and batteries. In: 2019 IEEE vehicle power and propulsion conference (VPPC); 2019. p. 1–7.

[24] Ettihir K, Boulon L, Agbossou K. Optimization-based energy management strategy for a fuel cell/battery hybrid power system. Appl Energy 2016;163:142–53.

[25] Tribioli L, Cozzolino R, Chiappini D, Iora P. Energy management of a plug-in fuel cell/battery hybrid vehicle with on-board fuel processing. Appl Energy 2016;184:140–54. https://doi.org/10.1016/j.apenergy.2016.10.015.

[26] Hou C, Ouyang M, Xu L, Wang H. Approximate pontryagin's minimum principle applied to the energy management of plug-in hybrid electric vehicles. Appl Energy 2014;115:174–89. https://doi.org/10.1016/j.apenergy.2013.11.002.

[27] Simmons K, Guezennec Y, Onori S. Modeling and energy management control design for a fuel cell hybrid passenger bus. J Power Sources 2014;246:736–46.

[28] Zheng CH, Xu GQ, Park YI, Lim WS, Cha SW. Prolonging fuel cell stack lifetime based on pontryagin's minimum principle in fuel cell hybrid vehicles and its economic influence evaluation. J Power Sources 2014;248:533–44. https://doi.org/10.1016/j.jpowsour.2013.09.110.

[29] Zhang S, Hu X, Xie S, Song Z, Hu L, Hou C. Adaptively coordinated optimization of battery aging and energy management in plug-in hybrid electric buses. Appl Energy 2019;256:113891.

[30] Song Z, Zhang X, Li J, Hofmann H, Ouyang M, Du J. Component sizing optimization of plug-in hybrid electric vehicles with the hybrid energy storage system. Energy 2018;144:393–403. https://doi.org/10.1016/j.energy.2017.12.009.

[31] Liu C, Liu L. Optimal power source sizing of fuel cell hybrid vehicles based on pontryagin's minimum principle. Int J Hydrogen Energy 2015;40(26):8454–64. https://doi.org/10.1016/j.ijhydene.2015.04.112.

[32] Zheng C, Xu G, Xu K, Pan Z, Liang Q. An energy management approach of hybrid vehicles using traffic preview information for energy saving. Energy Convers Manage 2015;105:462–70. https://doi.org/10.1016/j.enconman.2015.07.061.

[33] Sánchez M, Delprat S, Hofman T. Energy management of hybrid vehicles with state constraints: A penalty and implicit hamiltonian minimization approach. Appl Energy 2020;260:114149.

[34] Kirk D. Optimal Control Theory: An Introduction, Dover Books on Electrical Engineering Series. Dover Publications; 2004.

[35] Sundstrom O, Guzzella L. A generic dynamic programming matlab function. In: 2009 IEEE Control Applications, (CCA) Intelligent Control, (ISIC); 2009. p. 1625–30.